Accepted Manuscript

A mechanochemical route to single phase Cu_2ZnSnS_4 powder

A. Ritscher, J. Just, O. Dolotko, S. Schorr, M. Lerch

PII: S0925-8388(16)30328-0

DOI: 10.1016/j.jallcom.2016.02.058

Reference: JALCOM 36669

To appear in: *Journal of Alloys and Compounds*

Received Date: 30 October 2015

Revised Date: 19 January 2016

Accepted Date: 6 February 2016

Please cite this article as: A. Ritscher, J. Just, O. Dolotko, S. Schorr, M. Lerch, A mechanochemical route to single phase Cu_2ZnSnS_4 powder, *Journal of Alloys and Compounds* (2016), doi: 10.1016/j.jallcom.2016.02.058.

A mechanochemical route to single phase Cu_2ZnSnS_4 powder

A. Ritscher[1,2], J. Just[2,3], O. Dolotko[4], S. Schorr[2, 5], M. Lerch* [1]

[1] *Institut für Chemie, Technische Universität Berlin, Straße des 17.Juni 135, 10623 Berlin, Germany*

[2] *Helmholtz-Zentrum Berlin für Materialien und Energie, Hahn-Meitner-Platz 1, 14109 Berlin, Germany*

[3] *Fachbereich C- Physik, Bergische Universität Wuppertal, Gaußstr. 20, 42119 Wuppertal, Germany*

[4] *Heinz Maier-Leibnitz Zentrum (MLZ), Technische Universität München, Lichtenbergstr.1, 85748 Garching, Germany*

[5] *Institut für Geologische Wissenschaften, Freie Universität Berlin, Malteserstr. 74, 12249 Berlin, Germany*

Keywords: CZTS powder, planetary ball mill, mechanochemical synthesis, neutron scattering, cation distribution, Rietveld refinement

Abstract

With respect to absorber materials in solar cells, Cu_2ZnSnS_4 (CZTS) has been a focus of interest in recent years. In this work, a new route leading to single phase CZTS powders is presented. For structural characterization X-ray and neutron powder diffraction measurements were performed. Further structural and compositional analysis of the CZTS powder was carried out by means of X-ray absorption near edge spectroscopy (XANES) and wavelength-dispersive X-ray spectroscopy (WDS). The obtained CZTS powder with an actual composition of $Cu_{2.00(4)}Zn_{1.02(2)}Sn_{0.99(2)}S_{4.00(8)}$ adopts the kesterite-type structure. A detailed cation distribution analysis using the average neutron scattering length method revealed a partial disorder of copper and zinc on the (2c) and (2d) sites.

1 Introduction

The quaternary chalcogenide Cu_2ZnSnS_4 recently gained attraction as a prospective absorber material for thin film photovoltaic applications. As it consists merely of earth-abundant, non-toxic and low-cost elements, it would be a suitable alternative to other chalcogenide-based absorber materials such as CdTe or CIGS ($CuIn_xGa_{(1-x)}Se_2$) that are currently used in thin films. It is a direct band gap p-type semiconductor with an optical band gap energy value of 1.5 eV and has a large absorption coefficient in the order of 10^{-4} cm^{-1} [1-3]. Up to now record efficiencies of CZTS-based thin films reached values up to 8.4% [4]. Yet, compared to the currently used chalcopyrite materials, efficiencies are significantly lower.

In order to enhance the quality and the efficiency of CZTS thin film photovoltaics it is necessary to gain a deeper insight into the absorber material. Systematic analysis of the semiconductor compound and its structural, chemical, and physical properties has been in the focus of interest in the last few years [5-10]. Due to the formation of secondary phases it is challenging to prepare phase-pure CZTS powder, which is important for detailed experiments concerning the correlations between structural and electronic properties. Consequently, the main motivation of the here-presented research is the development of a new chemical route for the synthesis of phase-pure stoichiometric kesterite powder and its structural characterization.

CZTS is a quaternary semiconductor belonging to the I_2-II-IV-VI_4 compound family. It adopts a tetragonal structure that can be derived from the zinc blende type by doubling the c-axis of the cubic sphalerite unit cell and by substituting the cations. A substitution scheme from binary ZnS to ternary Cu_2ZnSnS_4 is shown in Figure 1.

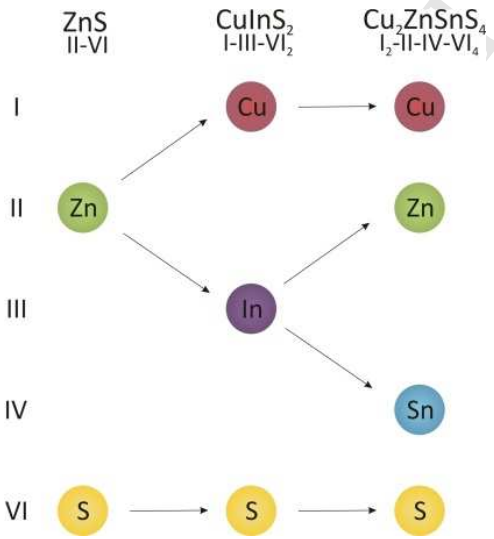

Figure 1 Cross-substitution steps from binary II-VI compound (ZnS) via ternary I-II-VI_2 ($CuInS_2$) to quaternary I_2-II-IV-VI_4 (Cu_2ZnSnS_4).

The correct crystal structure of CZTS has been a controversial issue. Two main structure types are described for quaternary $A^I{}_2B^{II}C^{IV}X^{VI}{}_4$ compounds, stannite (see Figure 2a) and kesterite (see Figure

2b) [11]. In these types the sulfur atoms form a ccp array where half of the tetrahedral voids are occupied by the cation species. The structures are closely connected but differ in the distribution of Cu^{+}, Zn^{2+}, and Sn^{4+}.

First reports on the crystal structure of natural specimen suggested the kesterite-type structure, space group $I\bar{4}$ (No. 82) [11], with a complete ordering of Cu^{+} and Zn^{2+}. Cu fully occupies the Wyckoff position 2a (0, 0, 0) whereas remaining Cu and Zn occupy the positions 2c (0, 1/2, 1/4) and 2d (0, 1/2, 3/4), respectively. Thus, the structure can be described by stacking cation layers Cu/Sn Cu/Zn Sn/Cu Cu/Zn Cu/Sn along the c-axis. Recently several groups could confirm that Cu_2ZnSnS_4 adopts the kesterite-type structure [5, 12, 13].

Using conventional X-ray diffraction methods, Cu^{+} and Zn^{2+} are not distinguishable due to their isoelectronic characteristic. As there is a significant difference in the neutron scattering length (b_{Cu}= 7.718(4) fm, b_{Zn}=5.680(5) fm), neutron diffraction is the method of choice. Neutron diffraction studies of Cu_2ZnSnS_4 powder samples confirm the kesterite-type structure, yet report a partial [14] or complete disorder [5] of Cu and Zn on the 2c and 2d positions. Kesterite-type phases exhibiting a statistical distribution of Cu/Zn can be described in space group $I\bar{4}2m$ (No. 121) with Zn and Cu occupying the 4d Wyckoff position (1/2, 0, 1/4) which is called disordered kesterite [15] (see Figure 2c).

It was also suggested by *ab initio* calculations [16, 17] that point defects Cu_{Zn} and Zn_{Cu} have very low formation energies, which underlines the possibility for Cu/Zn disorder. Recent studies on CZTS thin films determined the critical temperature for the transition from ordered to disordered kesterite to be at 260 ± 10 °C [18], which is also visible by a kink in the temperature dependent lattice parameter variation [6].

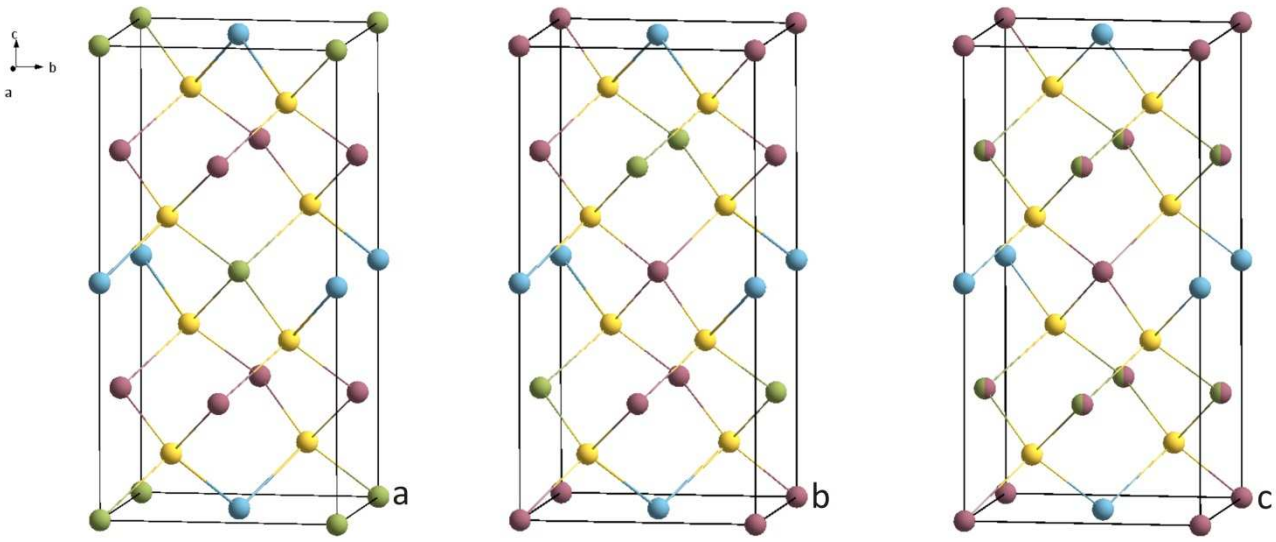

Figure 2 Unit cells of the (a) stannite, (b) kesterite, and (c) disordered kesterite structure; Cu(red) Zn(green) Sn(blue) S(yellow)

As four elements are present in the material, the formation of secondary phases such as CuS, Cu_2S, ZnS, SnS, SnS_2 and Cu_2SnS_3 seems probable. According to theoretical and experimental work [1, 19] the homogeneity region of the CZTS phase in the ternary phase diagram is rather small. Due to its small enthalpy of formation ZnS is likely to form and has been found to have a detrimental influence on solar cell performance. [7, 8, 20] Identification and quantification of the secondary phases ZnS and Cu_2SnS_3 by X-ray and neutron diffraction is difficult because of diffraction pattern overlap. As reported in [7] it is possible to identify the most important secondary phases with X-ray absorption spectroscopy (XAS).

In this study we investigate chemical composition and structural properties of a stoichiometric CZTS powder synthesized by a newly developed mechanochemical process. Phase purity and composition was determined by WDS and XANES. X-ray and neutron diffraction measurements were used to identify the crystal structure with a closer look to the cation distribution of the powder sample. Two refinement strategies will be discussed.

2 Experimental

2.1 Synthesis

The quaternary sulfide with the general formula Cu_2ZnSnS_4 was prepared by mechanical milling in a Fritsch Planetary Mono Mill PULVERISETTE 6 starting from the corresponding binary sulfides CuS, ZnS, and SnS followed by an annealing step.

Starting chemicals were prepared either by precipitation (CuS), sulfidation of the oxide (ZnS) or solid state reaction of the elements (SnS). Copper monosulfide (CuS) was precipitated from a 0.1 M $Cu(NO_3)_2$-solution (Merck, 99.5%) with H_2S (Air Liquide, 99.5%) and annealed at 230 °C in H_2S atmosphere for 2 h in a tube furnace. For the preparation of zinc sulfide (ZnS) reaction of the oxide ZnO (Merck, 99.5%) in a tube furnace with H_2S-gas at 650 °C for 3 h was performed. Tin monosulfide (SnS) was synthesized by a solid state reaction of the elements Sn (Merck, 99.9%) and S (Fluka, 99.99%) in an evacuated and sealed silica ampoule in a muffle furnace. Stoichiometric amounts of tin and sulfur were loaded in a silica ampoule. Due to the significant vapor pressure of sulfur the sealed and evacuated tube was first heated to 300 °C to avoid explosion. The temperature was increased to 800 °C with a rate of 15 °C/h and the sample was annealed for 30 h. According to [21] the compound was sublimed three times in the ampoule (750 °C → 550 °C) to ensure complete reaction. Identification of the binary compounds was done by powder X-ray diffraction.

For the synthesis of the quaternary sulfide the binary sulfides CuS, ZnS and SnS were mixed in an atomic ratio of 2:1:1 without any additional fluid medium and filled into an agate jar under Ar atmosphere in a glove box. A grinding bowl of 80 ml capacity is filled with 5 grinding balls with a diameter of 20 mm. Milling was performed in a high energy planetary ball mill using a rotational speed of 400 rpm and a milling time of 3 h with additional pauses of 30 min every hour to prevent the jar of heating up. The result of the mechanochemical treatment is a poorly crystalline product.

In order to get a well-crystalline product the sample was annealed in a conventional tube furnace equipped with a SiO_2-tube with an inner diameter of 70 mm in H_2S-atmosphere. The as-milled powder was placed in a small alumina boat inside the tube and heated under flowing reaction gas for 3 h at 500 °C. After reaction the sample was cooled down with a cooling rate of 60 K/h.

2.2 Characterization

The product was characterized both by X-ray and neutron powder diffraction. A Panalytical X'Pert PRO diffractometer (Bragg-Brentano geometry, Cu-Kα radiation) was used for powder XRD measurements. Neutron powder diffraction data were collected at the Forschungs-Neutronenquelle Heinz-Maier-Leibnitz Zentrum (MLZ, Garching) using the high resolution powder diffractometer SPODI (Ge (551) λ = 154.831 pm) [22]. For neutron experiments the sample was encapsulated in a vanadium container with 0.15mm wall thickness and 9 mm inner diameter (Ar atmosphere). Structural refinements were performed by the Rietveld method [23] using the program FULLPROF Suite Version 2015 [24] by applying a pseudo-Voigt [24] for the X-ray data and a Thompson-Cox-Hastings pseudo-Voigt function [25] for the neutron data, respectively.

Investigations of the chemical composition were performed by electron microprobe analysis (EMPA) with a JEOL JXA 8200 SuperProbe equipped with 5 wavelength dispersive X-ray spectrometers (WDS) and an energy dispersive X-ray spectrometer (EDS). X-ray absorption near edge structure measurements (XANES) at the sulfur K-edge (2472 eV) were carried out at the soft X-ray double crystal monochromator beamline KMC-1 at Bessy II (HZB) in transmission mode. The spectra were recorded with a pre-edge range of 70 eV and a range of 200 eV above the edge. Analysis of the spectra including energy calibration, background subtraction, normalization and fitting was performed with the IFEFFIT software package [26, 27].

In addition, possible contamination with nitrogen and oxygen were determined by a hot gas extraction with a LECO TC-300/EF-300 N/O analyzer. ZrO_2 and steel were used for calibration of the system (accuracy of N/O contents ~2%).

3 Results

3.1 Mechanochemical synthesis and annealing

Attempts to prepare single-phase CZTS have been met with varying levels of success. Up to this time, bulk material of the quaternary sulfide has been usually synthesized by solid state reactions of the pure elements in evacuated and sealed silica ampoules [5] according to the standard technique described in [28]. Due to the high sulfur vapor pressure it is necessary to apply a defined temperature program and homogenization is obtained by a second annealing step at 750 °C. All these factors result in a long reaction time and an enhanced possibility of the formation of secondary phases.

As mentioned in the introduction, the main motivation of our work is to develop a new chemical route for an easier and faster synthesis of phase-pure CZTS powder. The main idea is to create a formation

process where the annealing temperature of 750 °C is decreased in order to avoid thermal segregation and the formation of secondary phases. This can be realized by a mechanochemical approach and the synthesis of a precursor where the elements are already mixed at an atomic level. The first synthesis step is the reaction of the corresponding binary sulfides CuS, ZnS, and SnS in a high energy planetary ball mill as described in the experimental section.

Additionally, a time experiment following the reaction during the milling process was performed within a time range of 10 min to 180 min. During the milling process a small amount of powder was withdrawn at time intervals of 10-30 min from the grinding bowl. Selected diffraction patterns are depicted in Figure 3: after 10 minutes of milling the reflections of the binary sulfides are still present in the sample. After 3 hours of milling the reflections of the binary phases have vanished. Afterwards, the diffraction pattern did not change significantly, thus at this stage the powder was further processed.

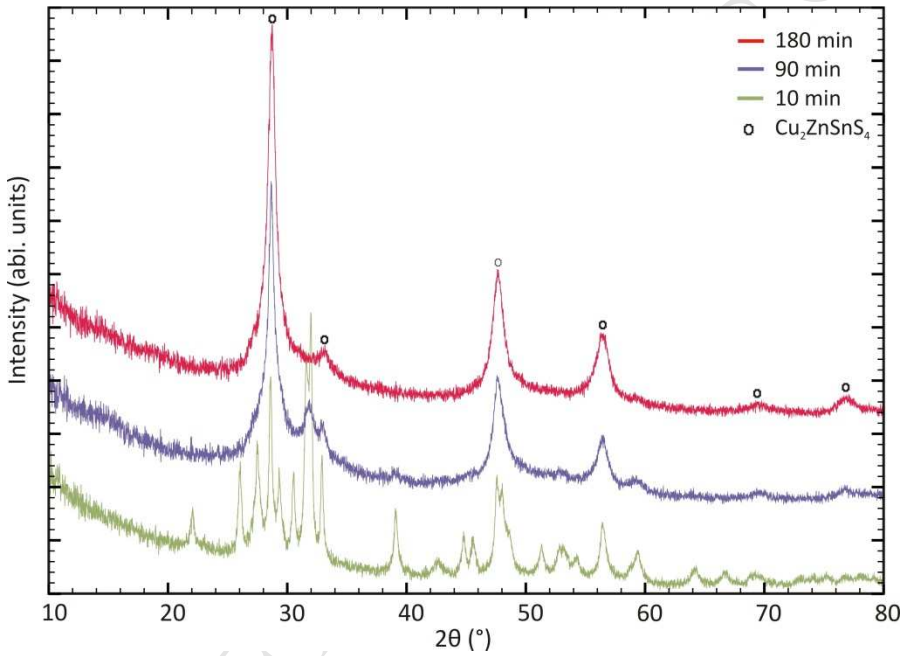

Figure 3 Diffraction patterns of samples milled for 10, 90, and 180 minutes, respectively.

In a second step the precursor powder is annealed in a tube furnace in H_2S atmosphere at 500 °C. This crystallization temperature is comparable to the temperature of actual thin film growth experiments which are often around 550 °C [29, 30]. The result of this annealing step is a product with good crystallinity. In Figure 4 the diffraction pattern of the as-milled sample as well as the crystalline sample after the annealing step is depicted. The crystal structure of the annealed sample was refined with the Rietveld method (for details see below). It should be mentioned that the milling step is essential for the synthesis of the above described quaternary sulfide. Annealing of the binary sulfides without a preceding milling process leads to the formation of secondary phases such as ZnS and SnS.

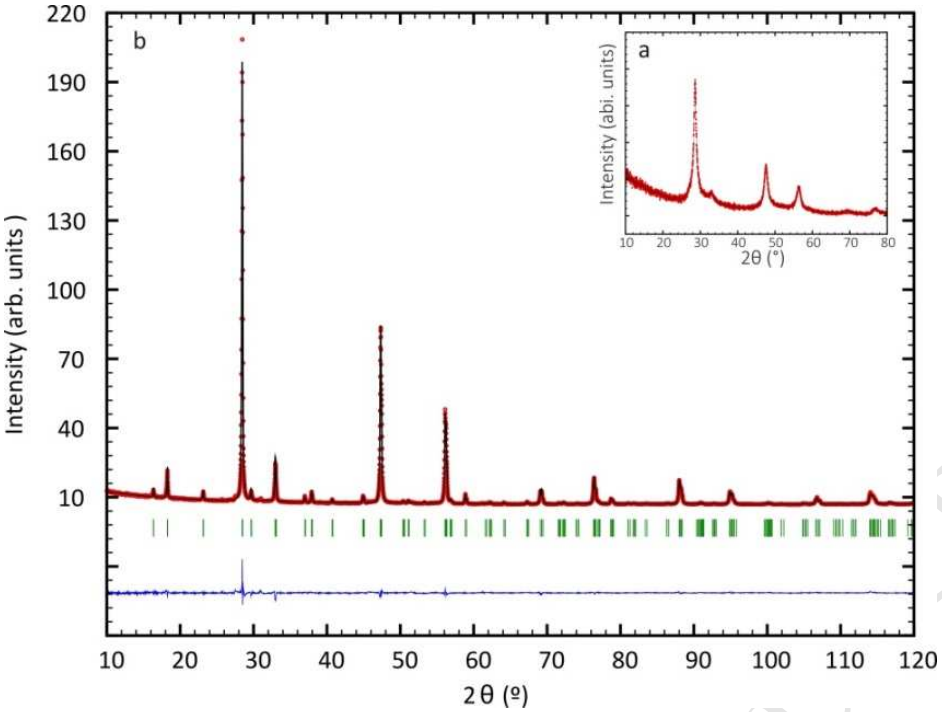

Figure 4 X-ray diffraction pattern of the as-milled (a) and annealed (b) CZTS sample together with the results of the Rietveld refinement (kesterite-type structure).

3.2 Chemical composition and phase purity

In order to determine the exact chemical composition of the synthesized sample, the powder was analyzed by WDS. A calibration of the microprobe system was done by using elemental standards in order to achieve reliable compositional parameters. High accuracy of the chemical composition could be obtained by measuring 50 grains of the CZTS phase averaging over 30 point measurements within each grain. The results of the phase analysis showed a homogenous composition, no secondary phases were found. The Cu/(Zn+Sn) and Zn/Sn ratio of the single phase CZTS sample were determined as 1.00 and 1.03, respectively, thus by taking into account the measurement error of the microprobe system the sample can be considered as stoichiometric, perhaps with a tendency of Zn excess resulting in a slight B-type off-stoichiometry (Figure 5). These off-stoichiometric models were first introduced in [31] and extended by [32]. Finally the integral chemical composition can be calculated as $Cu_{2.00(4)}Zn_{1.02(2)}Sn_{0.99(2)}S_{4.00(8)}$.

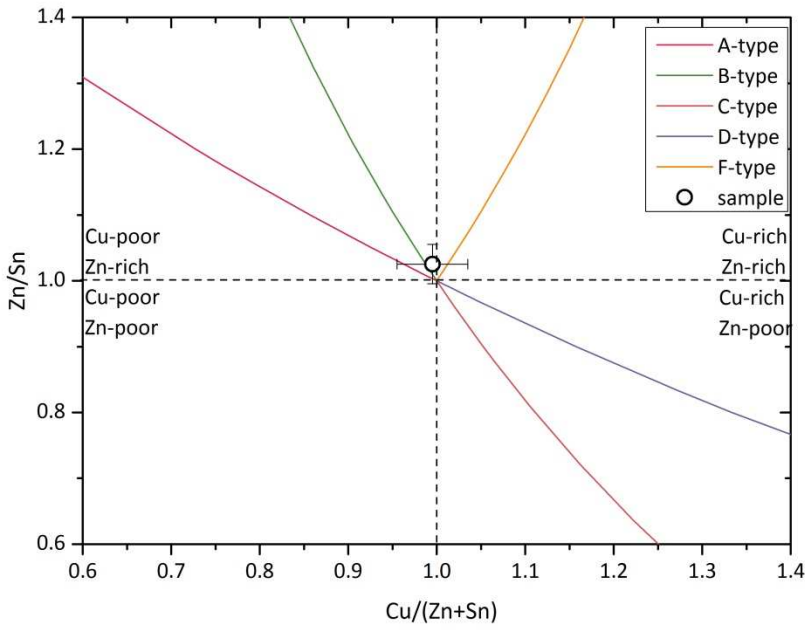

Figure 5 Cu/(Zn+Sn)-Zn/Sn plot showing the position of the mechanochemically prepared CZTS sample

Furthermore, phase purity was investigated by XANES. As explained in [7], X-ray absorption near edge structure analysis at the sulfur K-edge (2472 eV) gives information about the chemical environment of the selected atom, in this case sulfur, the electronic density of the unoccupied states, and the local crystal structure. It can be considered as a fingerprint for the identification of different materials [33]. The spectra of the binary phases CuS, ZnS, and SnS as well as that of CZTS are depicted in Figure 6. As already shown in [7] the spectra significantly differ from each other.

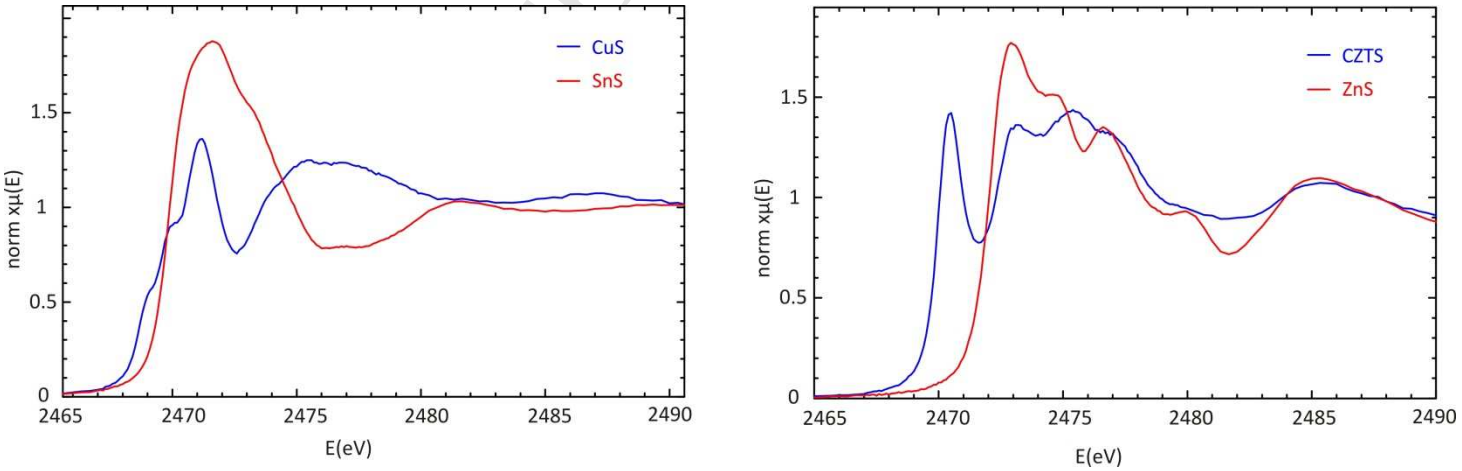

Figure 6 Edge step normalized XANES spectra at the sulfur K-edge of CZTS and corresponding binary sulfides

Therefore it is possible to identify secondary phases in CZTS samples. To perform a quantitative analysis of the secondary phases the measured spectrum was compared to a reference sample which can be assumed to be single phase CZTS and was already measured in [7]. The spectrum was fitted with a linear combination of the reference spectrum and the spectra of CuS, SnS, and ZnS. The

absolute error of the linear combination analysis depends on the fitting details as well as the reference sample purity and was estimated to be ± 3% [7]. Both spectra slightly differ around energies of 2469 eV and 2473 eV. The origin of these differences could so far not be identified. However, with linear combination analysis the presence of CuS, SnS or ZnS in significant amounts (> 3%) could be excluded. Additionally, in Figure 7 the CZTS sample is comparison with the CZTS reference sample is shown.

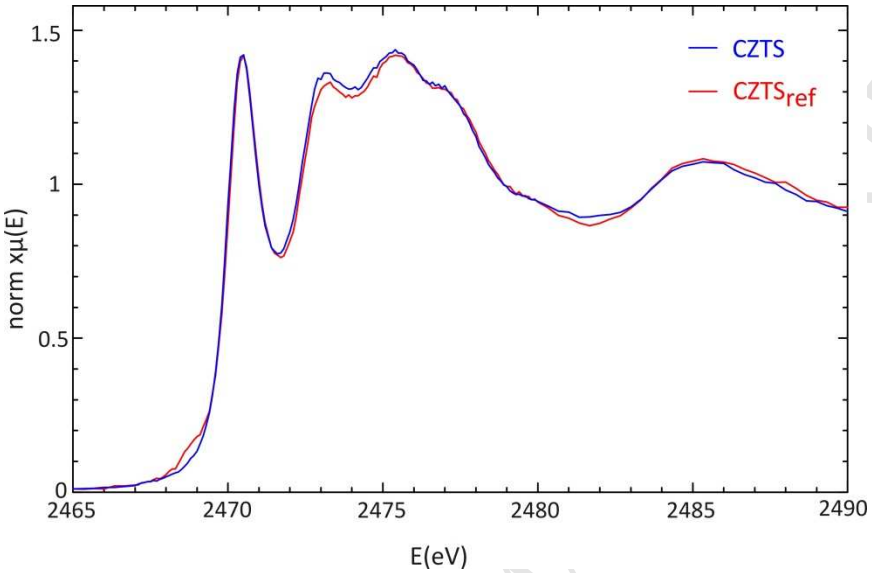

Figure 7 Measured and edge step normalized XANES spectra of the CZTS powder in comparison with the reference sample $CZTS_{ref}$

The results of the quantitative analysis by hot gas extraction showed that no significant amounts of nitrogen or oxygen are present in the sample.

3.3 Structural characterization

As mentioned above, the crystal structure of the synthesized black powder was refined with the help of the Rietveld method. As structural starting model we used the kesterite type (space group $I\bar{4}$). As the powder was detected to be stoichiometric within the standard deviation the stoichiometric composition Cu_2ZnSnS_4 was used for the structural refinement. The X-ray powder diffraction pattern with the results of the Rietveld refinement is depicted in Figure 4b. Looking at the difference plot it is obvious that refinement succeeded very well, thus the experimental data are in a very good agreement with the theoretical ones. Refined lattice parameters and residual values of the sample are summarized in Table 1.

Table 1 Lattice parameters and residual values of the Rietveld refinement of CZTS sample

	X-ray diffraction
Structure type	kesterite
Crystal system	tetragonal
Space group	$I\bar{4}$ (No.82)
Diffractometer	Panalytical X'Pert PRO
Wavelength	154.06 pm, 154.44 pm
2θ range	10-120 °
Z	2
a / pm	543.409(3)
c / pm	1084.210(11)
R_{Bragg} / %	3.89
R_{wp} / %	1.98
R_{exp} / %	1.07
S	1.85

As it is not possible to differentiate between Zn and Cu with conventional X-ray powder diffraction methods, this experiment can only be used to distinguish between Cu/Zn and Sn. Following constraints were applied:

- The stoichiometric composition Cu_2ZnSnS_4 was used
- The sum of Cu/Zn on all positions is 3
- The sum of Sn on all positions is 1
- Each cation position has a total occupancy of 1
- For the thermal motion an overall Debye-Waller factor was used

Table 2 lists the final atomic and additional structural parameters from the X-ray refinement. In conformity with literature data Sn was found on Wyckoff position 2b (0, 0, 1/2), whereas Cu/Zn is located on 2a (0, 0, 0), 2c (0, 1/2, 1/4) and 2d (0, 1/2, 3/4) sites. No Sn was found on positions 2a and 2c. However, around 3 % of Sn, that is present in the sample, is found on 2d site. Missing Sn on the 2b site is replaced by Cu/Zn.

Table 2 Refined structural parameters of CZTS from X-ray diffraction data. Occ for each cation position (2a, 2c, 2d, 2b) was constraint to 1. Values larger than 1 or below 0 are not meaningful and have to be considered as 1 and 0, respectively

Atom	**Wyckoff**	**x**	**y**	**z**	**B_{iso}***	**occ**
Cu/Zn	2a	0	0	0	0.991(9)	1.008(2)
Sn	2a	0	0	0	0.991(9)	-0.008(2)
Cu/Zn	2c	0	1/2	1/4	0.991(9)	1.001(9)
Sn	2c	0	1/2	1/4	0.991(9)	-0.001(9)
Cu/Zn	2d	0	1/2	3/4	0.991(9)	0.967(10)
Sn	2d	0	1/2	3/4	0.991(9)	0.033(10)
Cu/Zn	2b	0	0	1/2	0.991(9)	0.023(2)
Sn	2b	0	0	1/2	0.991(9)	0.977(2)
S	8g	0.755(3)	0.757(3)	0.8718(2)	0.991(9)	4

* not refined independently

Table 3 Lattice parameters and residual values of the Rietveld refinement from Neutron diffraction data

Neutron diffraction	**Strategy A**	**Strategy B**
Structure type	kesterite	
Crystal system	tetragonal	
Space group	$I\bar{4}$ (No.82)	
Diffractometer	SPODI	
Wavelength	154.83 pm	
2θ range	1-150 °	
a / pm	543.547(2)	543.547(2)
c / pm	1084.438(7)	1084.438(7)
R_{Bragg} / %	1.68	1.76
R_{wp} / %	2.45	2.45
R_{exp} / %	1.62	1.62
S	1.51	1.51

With the aim to reveal also the copper/zinc cation ordering on the four crystallographic sites, neutron diffraction measurements of the product were performed. Two strategies for the refinement were tested.

Strategy A:

- The stoichiometric composition Cu_2ZnSnS_4 was applied
- The sum of Cu on all positions is 2
- The sum of Zn on all positions is 1
- The values of Sn were adopted to the values of the XRD-refinement and not refined
- Each cation position has a total occupancy of 1

As described above, the occupancy values for Sn were fixed to the values obtained from our X-ray refinement (Wyckoff positions 2d and 2b) whereas the occupancy values of Cu and Zn were refined on positions 2a (0, 0, 0), 2c (0, 1/2, 1/4), 2d (0, 1/2, 3/4) and 2b (0, 0, 1/2). The neutron powder diffraction pattern together with the results of the Rietveld refinements is depicted in Figure 8. The final atomic and additional structural parameters are summarized in Table 4. Looking at the site occupancy factors it can be seen that the 2a site is primarily occupied by Cu with small amounts of additional Zn. However, within the error of the refinement the Zn content on this position can be considered as zero. Cu is also the dominant element on the 2c site whereas the 2d position is mainly occupied with Zn. This is in good agreement with the literature data of ordered kesterite phases where Cu fully occupies the 2c and Zn the 2d position. No Zn was found on the 2b site. This is summarized in Fig. 8.

Table 4 Refined structural parameters from neutron diffraction data (strategy A). *refined values from X-ray diffraction data

Atom	Wyckoff	x	y	z	B_{iso}	occ
Cu	2a	0	0	0	2.28(10)	0.97(4)
Zn	2a	0	0	0	2.28(10)	0.04(4)
Cu	2c	0	1/2	1/4	0.9(2)	0.75(7)
Zn	2c	0	1/2	1/4	0.9(2)	0.25(7)
Cu	2d	0	1/2	3/4	0.6(2)	0.26(4)
Zn	2d	0	1/2	3/4	0.6(2)	0.71(4)
Sn	2d	0	1/2	3/4	0.6(2)	0.033*
Cu	2b	0	0	1/2	0.92(8)	0.023(9)
Zn	2b	0	0	1/2	0.92(8)	0.001(9)
Sn	2b	0	0	1/2	0.92(8)	0.977*
S	8g	0.758(2)	0.751(3)	0.8756(10)	0.85(3)	4

Strategy B:

As a second approach the method of the average neutron scattering length, which was introduced by Schorr [34] for determination of the cation distribution of different semiconductor compounds, was applied (strategy B). For this refinement the slight off-stoichiometric composition $Cu_{2.00(4)}Zn_{1.02(2)}Sn_{0.99(2)}S_{4.00(8)}$ was used. As starting model the cations were distributed on the four lattice sites as follows: Cu on the Wyckoff positions 2a (0, 0, 0) and 2c (0, 1/2, 1/4), Zn on 2d (0, 1/2, 3/4) and Sn on 2b (0, 0, 1/2). Refined parameters are summarized in Table 5. The neutron powder diagram together with the results of the Rietveld refinements is depicted in Figure 8.

Table 5 Refined structural parameters from neutron diffraction data (strategy B)

Atom	Wyckoff	x	y	z	B_{iso}	occ
Cu	2a	0	0	0	2.33(10)	1.02(2)
Cu	2c	0	1/2	1/4	0.8(2)	0.91(3)
Zn	2d	0	1/2	3/4	0.7(2)	1.11(4)
Sn	2b	0	0	1/2	0.96(8)	1.01(2)
S	8g	0.750(3)	0.758(2)	0.8757(10)	0.83(3)	4

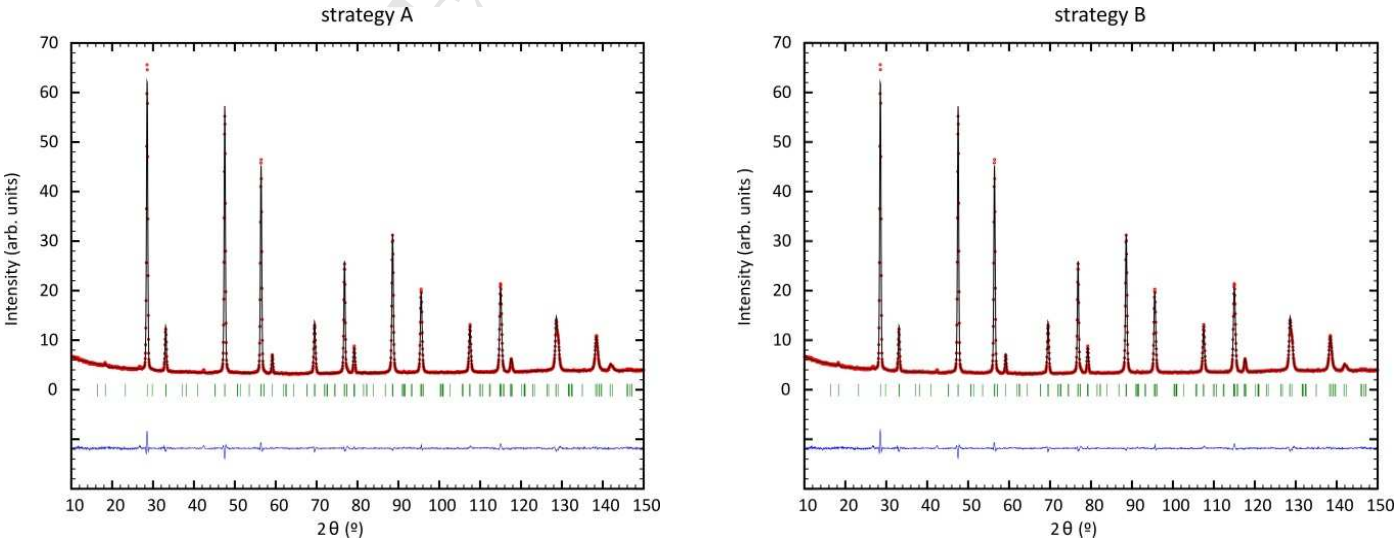

Figure 8 Neutron powder diffraction pattern with results of Rietveld refinements using the kesterite-type structure as starting model. (left- strategy A, right- strategy B)

The refined site occupancies are used to calculate the experimental average neutron scattering lengths according to Equation 1.

Equation 1

$$\bar{b}_{2a}^{\ exp} = occ_{2a} \cdot b_{Cu}$$
$$\bar{b}_{2c}^{\ exp} = occ_{2c} \cdot b_{Cu}$$
$$\bar{b}_{2d}^{\ exp} = occ_{2d} \cdot b_{Zn}$$
$$\bar{b}_{2b}^{\ exp} = occ_{2b} \cdot b_{Sn}$$

where $\bar{\boldsymbol{b}}^{\boldsymbol{exp}}$ is the experimental determined average neutron scattering length of the site, *occ* the occupancy of the respective site, and *b* is the scattering length of the particular cation (b_{Cu} = 7.718 fm, b_{Zn} = 5.680 fm, b_{Sn} = 6.225 fm).

The obtained values for the average neutron scattering lengths are compared with the neutron scattering lengths of Cu, Zn and Sn. An occurring deviation from the initial value shows that the cation sites 2c and 2d are not exclusively occupied by the presumed atom. For the calculation of the cation distribution Equation 2 is used.

Equation 2

$$\bar{b}_i = X_i \cdot b_{Cu} + Y_i \cdot b_{Zn} + Z_i \cdot b_{Sn}$$

where $\bar{\boldsymbol{b}}_{\boldsymbol{i}}$ is the average neutron scattering length of site *i* (2a, 2c, 2d, 2b), X_i, Y_i and Z_i the fraction of Cu, Zn and Sn on the respective site, and *b* is again the scattering length of the cation. In the global optimization procedure all values were simultaneously optimised and the following conditions have to be fulfilled: minimisation of the difference between $\bar{\boldsymbol{b}}^{\boldsymbol{exp}}$ and $\bar{\boldsymbol{b}}_{\boldsymbol{i}}$; each position is fully occupied; there is no deviation from the given stoichiometry.

From strategy B following supposition can be made: 2a is fully occupied by copper. The average neutron scattering length of the 2c site is significantly lower than compared to full occupancy with Cu, suggesting the presence of Zn_{Cu} or Sn_{Cu} antisites. However, significant amounts of Sn_{Cu} antisites on the 2c site were excluded by the X-ray refinement. An indication for Cu_{Zn} antisites is suggested on the 2d site due to the significantly higher average neutron scattering length compared to the value of Zn. The value for Sn on the 2b site would suggest that only Sn is present on this position. All this is summarized in Figure 9.

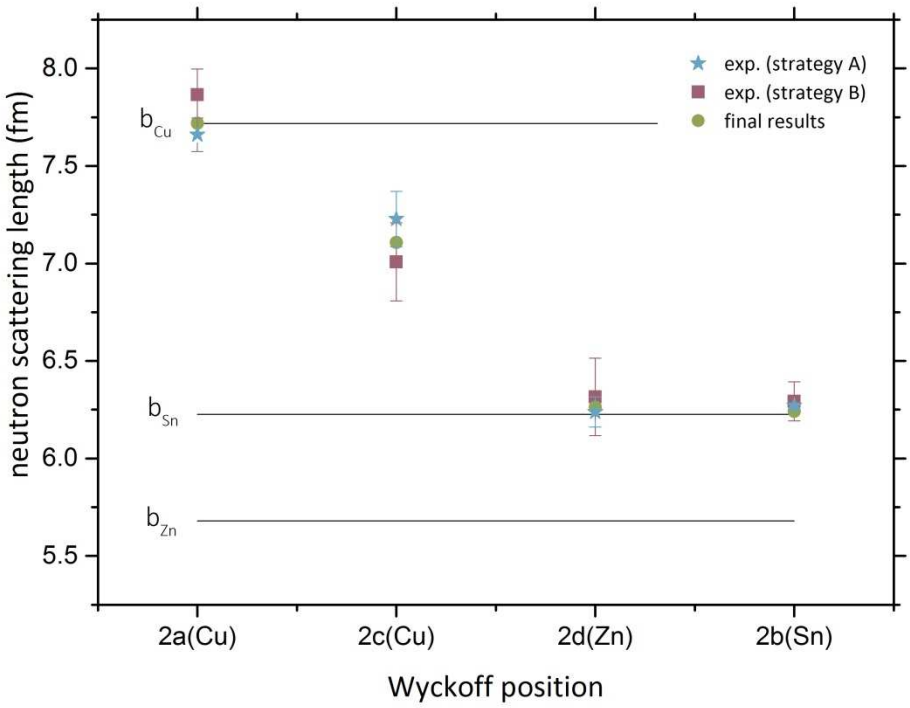

Figure 9 Experimentally determined values of the average neutron scattering length $\bar{b}$ of the 2a, 2c, 2d and 2b sites for strategy A and B and final values resulting from both strategies

From the results presented in Table 3 it is obvious that both refinements succeeded very well. Comparing the lattice parameters, residual values and structural parameters no significant differences are observed. However, two deviations of the results of both refinements have to be mentioned. Zn was found in the amount of 4% on the 2a site in strategy A whereas in strategy B no Zn was found on this position. By taking into account the error of the refined parameter Zn_{2a} in strategy A the Zn content can be considered as zero though. Secondly, Sn_{Zn} of ~2% are found on the 2d site in strategy A, assuming a stoichiometric composition Cu_2ZnSnS_4. Using the composition $Cu_{2.00(4)}Zn_{1.02(2)}Sn_{0.99(2)}S_{4.00(8)}$ in strategy B, the entire amount of Sn is on the 2b site.

In Figure 9 the experimentally determined average neutron scattering lengths for the cation sites for both refinement strategies and the calculated values ($\bar{b}_i$) are compared. It can be easily seen that the values for both strategies are in good agreement with each other.

Independently from the refinement strategy the following statements can be made: cation site 2a is fully occupied by copper. On the 2c site the presence of Zn_{Cu} antisites is clearly seen (~28%). An additional indication comes from the occupancy factors of the 2d site (presence of Cu_{Zn} in the order of ~28%). The determined values for the 2b site suggest that within the experimental error this site is only occupied by tin. This is summarized in Figure 9 and Figure 10.

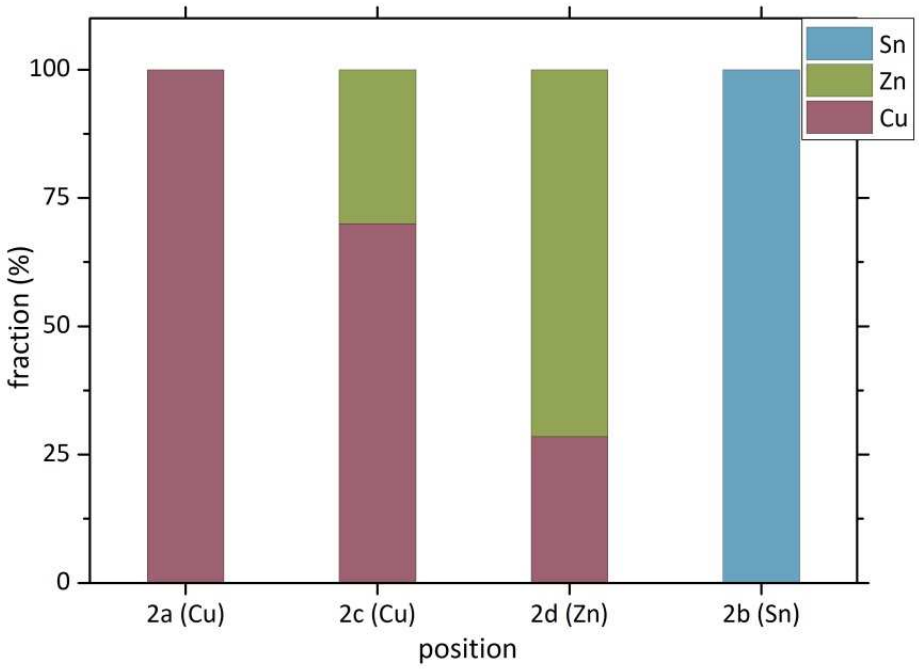

Figure 10 Cation distribution of the synthesized sample

4 Conclusions

A mechanochemical synthesis route to CZTS was successfully developed. The synthesis process includes a milling step, which is essential to produce phase pure powder, and an annealing step at 500 °C. This reaction temperature is favorable as it is comparable to the temperatures actually used during thin films growth and is close to the real technical process conditions.

WDS measurements confirmed a stoichiometric chemical composition of $Cu_{2.00(4)}Zn_{1.02(2)}Sn_{0.99(2)}S_{4.00(8)}$ and no secondary phases were found in XANES. The results of diffraction studies showed that the powder crystallizes in the kesterite-type structure. The cation distribution was determined by neutron powder diffraction measurements and revealed a partially disordered kesterite type. The ordering of the cations should significantly depend on the cooling rate of the sample during preparation. For different cooling procedures we expect a differing distribution of the cations. In order to investigate this phenomenon, additional neutron scattering experiments are scheduled.

With the developed mechanochemical route it is nicely possible to control the composition of the synthesized powder. Therefore, additional experiments to prepare phase-pure off-stoichiometric CZTS material are planned.

Acknowledgement

The authors thank C. Behr, PD Dr. R. Milke (FU Berlin), and K. Neldner (HZB) for support with the microprobe analyses. Financial support from the MatSEC graduate school of the Helmholtz Zentrum Berlin (HZB) in cooperation with the Dahlem Research School is gratefully acknowledged.

References

[1] S. Chen, X.G. Gong, A. Walsh, S.-H. Wei, Crystal and electronic band structure of Cu_2ZnSnX_4 (X=S and Se) photovoltaic absorbers: First-principles insights, Appl. Phys. Lett., 94 (2009) 041903/041901-041903/041903.
[2] J.J. Scragg, P.J. Dale, L.M. Peter, G. Zoppi, I. Forbes, New routes to sustainable photovoltaics: evaluation of Cu_2ZnSnS_4 as an alternative absorber material, Phys. Status Solidi B, 245 (2008) 1772-1778.
[3] S. Siebentritt, S. Schorr, Kesterites - a challenging material for solar cells, Prog. Photovoltaics, 20 (2012) 512-519.
[4] B. Shin, O. Gunawan, Y. Zhu, N.A. Bojarczuk, S.J. Chey, S. Guha, Thin film solar cell with 8.4% power conversion efficiency using an earth-abundant Cu_2ZnSnS_4 absorber, Prog. Photovoltaics, 21 (2013) 72-76.
[5] S. Schorr, H.-J. Hoebler, M. Tovar, A neutron diffraction study of the stannite-kesterite solid solution series, Eur. J. Mineral., 19 (2007) 65-73.
[6] S. Schorr, G. Gonzalez-Aviles, In-situ investigation of the structural phase transition in kesterite, Phys. Status Solidi A, 206 (2009) 1054-1058.
[7] J. Just, D. Luetzenkirchen-Hecht, R. Frahm, S. Schorr, T. Unold, Determination of secondary phases in kesterite Cu_2ZnSnS_4 thin films by x-ray absorption near edge structure analysis, Appl. Phys. Lett., 99 (2011) 262105/262101-262105/262103.
[8] S. Chen, X.G. Gong, A. Walsh, S.-H. Wei, Defect physics of the kesterite thin-film solar cell absorber Cu_2ZnSnS_4 Appl. Phys. Lett., 96 (2010) 021902/021901-021902/021903.
[9] S. Chen, L.-W. Wang, A. Walsh, X.G. Gong, S.-H. Wei, Abundance of CuZn+SnZn and 2CuZn+SnZn defect clusters in kesterite solar cells, Appl. Phys. Lett., 101 (2012) 223901/223901-223901/223904.
[10] A.J. Jackson, A. Walsh, Ab initio thermodynamic model of Cu_2ZnSnS_4 J. Mater. Chem. A, (2014) 7829-7836.
[11] S.R. Hall, J.T. Szymanski, J.M. Stewart, Kesterite, $Cu_2(Zn,Fe)SnS_4$, and stannite, $Cu_2(Fe,Zn)SnS_4$, structurally similar but distinct minerals Can. Mineral., 16 (1978) 131-137.
[12] S. Schorr, The crystal structure of kesterite type compounds: A neutron and X-ray diffraction study, Sol. Energy Mater. Sol. Cells, 95 (2011) 1482-1488.
[13] L. Choubrac, A. Lafond, C. Guillot-Deudon, Y. Moelo, S. Jobic, Structure Flexibility of the Cu_2ZnSnS_4 Absorber in Low-Cost Photovoltaic Cells: From the Stoichiometric to the Copper-Poor Compounds, Inorg. Chem., 51 (2012) 3346-3348.
[14] S. Schorr, M. Tovar, Bensc 2006_Review, BENSC Experimental Report, (2006).
[15] M.Y. Valakh, V.M. Dzhagan, I.S. Babichuk, X. Fontane, A. Perez-Rodriquez, S. Schorr, Optically induced structural transformation in disordered kesterite Cu_2ZnSnS_4 JETP Lett., 98 (2013) 255-258.
[16] A. Nagoya, R. Asahi, R. Wahl, G. Kresse, Defect formation and phase stability of Cu_2ZnSnS_4 photovoltaic material, Phys. Rev. B Condens. Matter Mater. Phys., 81 (2010) 113202/113201-113202/113204.
[17] S. Chen, J.-H. Yang, X.G. Gong, A. Walsh, S.-H. Wei, Intrinsic point defects and complexes in the quaternary kesterite semiconductor Cu_2ZnSnS_4 Phys. Rev. B: Condens. Matter Mater. Phys., 81 (2010) 245204/245201-245204/245210.
[18] J.J.S. Scragg, L. Choubrac, A. Lafond, T. Ericson, C. Platzer-Bjoerkman, A low-temperature order-disorder transition in Cu_2ZnSnS_4 thin films, Appl. Phys. Lett., 104 (2014) 041911/041911-041911/041914.
[19] I.D. Olekseyuk, I.V. Dudchak, L.V. Piskach, Phase equilibria in the Cu_2S-ZnS-SnS_2 system J. Alloys Compd., 368 (2004) 135-143.
[20] J. Timo Waetjen, J. Engman, M. Edoff, C. Platzer-Bjoerkman, Direct evidence of current blocking by ZnSe in $Cu_2ZnSnSe_4$ solar cells, Appl. Phys. Lett., 100 (2012) 173510/173511-173510/173513.
[21] H. Wiedemeier, F.J. Csillag, Equilibrium sublimation and thermodynamic properties of tin(II) sulfide, Thermochim. Acta, 34 (1979) 257-265.

[22] M. Hoelzel, A. Senyshyn, N. Juenke, H. Boysen, W. Schmahl, H. Fuess, High-resolution neutron powder diffractometer SPODI at research reactor FRM II, Nucl. Instrum. Methods Phys. Res., Sect. A, 667 (2012) 32-37.
[23] H.M. Rietveld, Profile refinement method for nuclear and magnetic structures, J. Appl. Crystallogr., 2 (1969) 65-71.
[24] J. Rodriguez-Carvajal, Abstracts of the Satellite Meeting on Powder Diffraction of the XV.Congress of the IUCr, (1990) 127.
[25] P. Thompson, D.E. Cox, J.B. Hastings, Rietveld refinement of Debye-Scherrer synchrotron X-ray data from alumina, J. Appl. Crystallogr., 20 (1987) 79-83.
[26] M. Newville, IFEFFIT: interactive XAFS analysis and FEFF fitting, J. Synchrotron Radiat., 8 (2001) 322-324.
[27] B. Ravel, M. Newville, ATHENA, ARTEMIS, HEPHAESTUS: data analysis for x-ray absorption spectroscopy using IFEFFIT, J. Synchrotron Radiat., 12 (2005) 537-541.
[28] G.P. Bernardini, P. Bonazzi, M. Corazza, F. Corsini, G. Mazzetti, L. Poggi, G. Tanelli, New data on the Cu_2FeSnS_4 -Cu_2ZnSnS_4 pseudobinary system at 750° and 550°C Eur. J. Mineral., 2 (1990) 219-225.
[29] J.J. Scragg, T. Ericson, X. Fontane, V. Izquierdo-Roca, A. Perez-Rodriguez, T. Kubart, M. Edoff, C. Platzer-Bjoerkman, Rapid annealing of reactively sputtered precursors for Cu_2ZnSnS_4 solar cells, Prog. Photovoltaics, 22 (2014) 10-17.
[30] B.-A. Schubert, B. Marsen, S. Cinque, T. Unold, R. Klenk, S. Schorr, H.-W. Schock, Cu_2ZnSnS_4 thin film solar cells by fast coevaporation, Prog. Photovoltaics, 19 (2011) 93-96.
[31] A. Lafond, L. Choubrac, C. Guillot-Deudon, P. Deniard, S. Jobic, Crystal Structures of Photovoltaic Chalcogenides, an Intricate Puzzle to Solve: the Cases of CIGSe and CZTS Materials, Z. Anorg. Allg. Chem., 638 (2012) 2571-2577.
[32] L.E. Valle-Rios, K. Neldner, G. Gurieva, S. Schorr, Existence of off-stoichiometric single phase kesterite, J. Alloys Comp., 657 (2016) 408-413.
[33] D.C. Koningsberger, R. Prins, X-ray Absorption: Principles, Applications, Techniques of EXAFS SEXAFS, and XANES, John Wiley & Sons, 1988.
[34] S. Schorr, C. Stephan, T. Toerndahl, R. Mainz, X-ray and neutron diffraction on materials for thin-film solar cells, in, Wiley-VCH Verlag GmbH & Co. KGaA, 2011, pp. 347-363.

Highlights

Mechanochemical synthesis of phase pure kesterite powder.

Determination of the cation distribution using neutron diffraction.

Partial disorder for copper and zinc observed.